An Arctic ship performance model for sea routes in ice-infested waters

Christopher Ryan[a], Luofeng Huang[a, *], Zhiyuan Li[b, *], Jonas W. Ringsberg[b], Giles Thomas[a]

[a]Department of Mechanical Engineering, University College London, United Kingdom

[b]Department of Mechanics and Maritime Science, Chalmers University of Technology, Sweden

Abstract: Global warming is creating significant change in the Arctic environment, with widespread reduction in ice extent, thickness and compactness. This has opened numerous shipping routes through the Arctic and provides the opportunity to reduce the distance, time and emissions of voyages. However, for a ship to operate in such polar routes, ice conditions need to be properly accounted for to accurately estimate fuel consumption. To meet this key challenge, this paper presents a ship performance model that was designed to incorporate a set of ice resistance algorithms alongside the calculation of open-water ship resistance and fuel consumption. In particular, a novel method is proposed to calculate ship resistance in ice-floe fields, other than the traditional level-ice condition. Subsequently, the model was used to simulate a voyage in the Northern Sea Route and the fuel consumption prediction agreed well with corresponding full-scale measurement data. Overall, the work provided a practical tool for the emerging Arctic shipping industry to carry out fuel analysis and voyage planning.

Keywords: Arctic, ship performance model, ice floe, ice resistance, fuel consumption.

1. Introduction

Climate change has caused the Arctic sea ice to melt dramatically, in turn causing a transition from extensive ice coverage to mostly open water. The changing conditions make the Arctic more accessible to ships, with new waterways allowing improved access for oil and gas extraction, mining, fishing and tourism. In addition, two major transit shipping routes are now becoming viable: the Northwest Passage (NWP) and the Northern Sea Route (NSR), which are considered alternatives to the Panama and Suez canals to connect Europe, Asia and America. Compared with current routes, both of these new routes can reduce travel distance by up to 40%, leading to substantial fuel, cost, time and emission savings [1] as illustrated in Figure 1.

*Corresponding authors: ucemlhu@ucl.ac.uk (L. Huang), zhiyuan.li@chalmers.se (Z. Li)

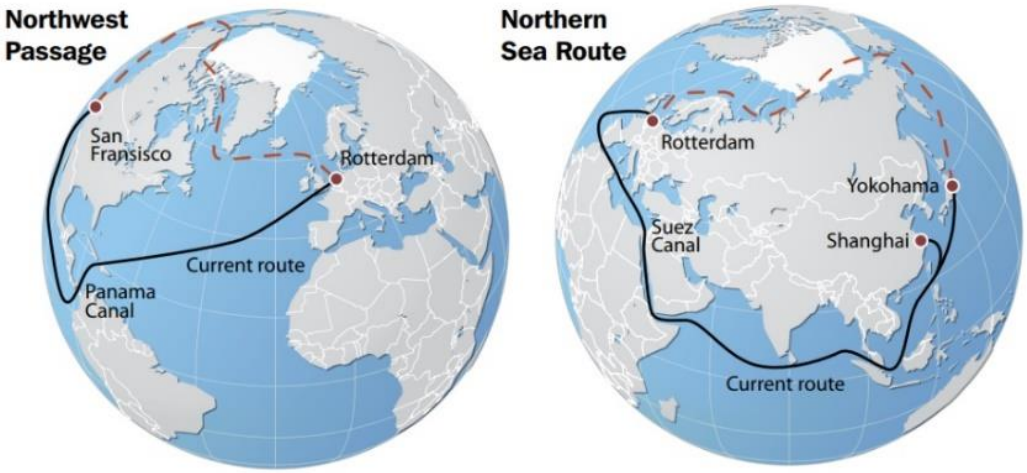

Figure 1: Comparison between the Arctic shipping routes (red dash lines) and the traditional shipping routes (black solid lines) [2]

The opportunities presented by this change in Arctic conditions are attracting significant research interest in Arctic shipping. One of the significant research challenges in this area is to accurately predict engine power requirements and fuel consumption for the new routes that are still affected by seasonally and regionally varying sea ice. This requires a Ship Performance Model (SPM) that can assess the resistance and fuel consumption of a given ship in a given voyage condition, enabling the comparison of resistance between different hull forms, as well as the comparison of different routes [3,4]; such an SPM is required to accurately account for the effect of different ice conditions on ship resistance. Contemporary SPMs have been widely built for open-ocean sailing estimates and optimisation, while they are not ready for the Arctic case due to the exclusion of ice resistance components. Examples of open water ship performance models are those developed by Calleya [5] and Tillig [6].

To account for the effect of ice on ship performance, models are required for the ship-ice interactions. Traditionally, ship-ice interaction models have focused on the level-ice condition, as the Arctic region tended to be covered by consolidated ice all year round and was only accessible to icebreakers. A large number of models were developed to formulate the ice-breaking process so as to predict the effect of level ice on ship resistance [7–9]. These models have been widely applied in practice and have evolved into international guidelines, such as the Finnish-Swedish Ice Class Rules (FSICR) [10].

The emerging Arctic voyage conditions appear to be more complex than just open water or level-ice coverage however. Other than those two scenarios, the melted ice cover can also develop into numerous ice floes floating on the sea surface. As a transition between level ice and open water, the floe-ice condition has been predicted to be the most prevalent sea ice condition in the future Arctic [11]. These

ice floes, also known as pancake ice, tend to be circular under the effect of wave wash and floe–floe collisions.

Figure 2 demonstrates the dominance of the ice-floe condition (green and blue) along Arctic shipping routes, reported by field observations in the autumn of 2015, while level ice (red) only occupies a small portion. With global warming, it can be anticipated that the proportion of ice-floe conditions will continue increasing, and the average size of floes will decrease. The emerging ice-floe conditions are navigable for commercial ships without ice-breaking capabilities, as shown in Figure 3, despite requiring icebreaker assistance when encountering level ice. Along with this changing ice condition, a significant increase in navigable days for open-water vessels is envisioned to be ongoing for both NWP and NSR [12]. Therefore, shipping in such small floating ice floes is becoming a principal Arctic shipping scenario. As a fact, traffic through the icy region's busiest lane along the Siberian coast increased 58% between 2016 and 2019; in 2020, ships made 2,694 voyages on the NSR, according to data collection of the Centre for High North Logistics at Norway's Nord University [13].

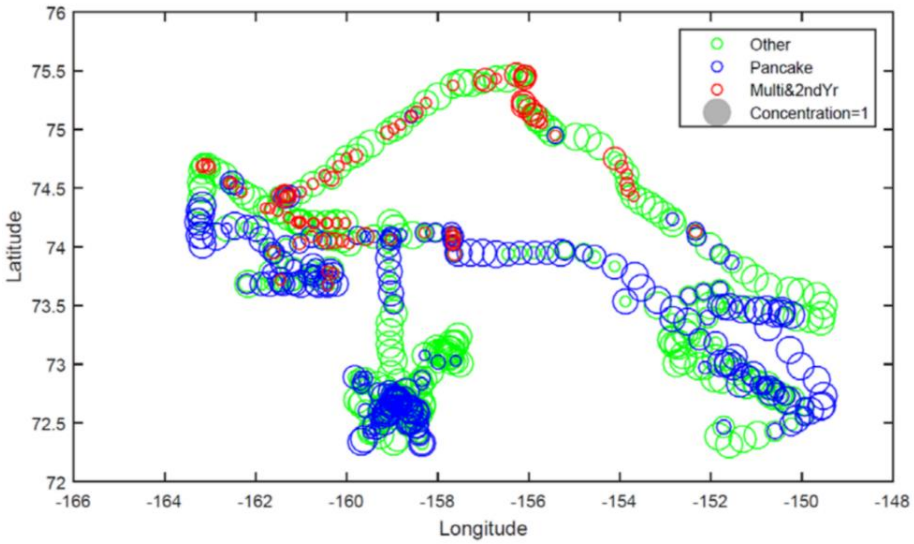

Figure 2: Ice floes (pancake and other) observed as the primary environment of shipping routes in the Western Arctic [11]; the different circle sizes indicate the ice concentration, relative to the grey circle in the top-right legend that represents concentration = 1; The X and Y axes indicate geographical locations by Longitude and Latitude (in terms of degree).

Figure 3: A non-icebreaking vessel operating in small ice-floe condition infested on the NSR (photo credit: SCF Group)

Experimental work on the ship interaction with small floating ice floes has been widely conducted. In this scenario, advancing ships tend to push the floes aside rather than break them [14], thus most experiments applied rigid polymer materials to mimic the ice floes [15–17]. Real ice experiments have also been performed by Kim et al. [18] according to field measurements of the relative dimensions between the ship and floes, which confirmed that the ice floes occur negligible fracture in this case. Nonetheless, when the ice floe size is sufficiently large, ship-induced ice fracture will occur and this requires to be investigated separately due to the changed physics [19]. In addition, measurements have been conducted for assessing the floe-induced force on a moored ship structure [20,21]; however, as the examined ice speed conditions are very small compared with normal shipping speeds, the results for moored structures cannot be directly applied to ship resistance in ice floes. Generally, relevant experimental data are still scarce due to the prohibitive costs and complexity of ice experiments involving parameter matrices.

To provide a cost-effective approach, discrete/finite element simulation has been a standard method applied to simulate the operation of ships in scattered ice floes [22–27]. However, one significant gap was to accurately account for the force of the surrounding fluid on the ice, which was usually implemented by empirical equations [28]. Due to this deficiency, previous simulations of a ship advancing in ice floes ignored the effect of fluid flow, i.e. ship-generated waves, which reduces the reality of the modelling. The process of a ship advancing in floating ice floes can be summarised as the following ship-wave-ice interaction: ship advancement generates waves; waves interact with ice floes; ice floes contact each other and with the ship [29–32]. The ship-generated waves can play a key role within the process; for example, the wave can change the velocity (magnitude and direction) of floes,

especially when the floes are small. Therefore, ignoring the wave effect may considerably influence the ice load on a ship.

To account for the ship-generated wave in the modelling process, Huang et al. [33] proposed a computational method that can simulate the operation of ships in ice floes. This method used a combined CFD & DEM (Computational Fluid Dynamics and Discrete Element Method) approach to solve this problem. The ship and wave dynamics are obtained using CFD, while ice behaviours are solved by DEM and coupled with CFD. This method enabled the simulation of the floe ice scenario with high-fidelity, as shown in Figure 4, and its accuracies have been validated against experiments. Huang et al. [34] then proposed a regression procedure that can derive empirical equations from the simulation ready to be incorporated into an SPM. This innovation provides the possibility to establish an integrated Arctic SPM.

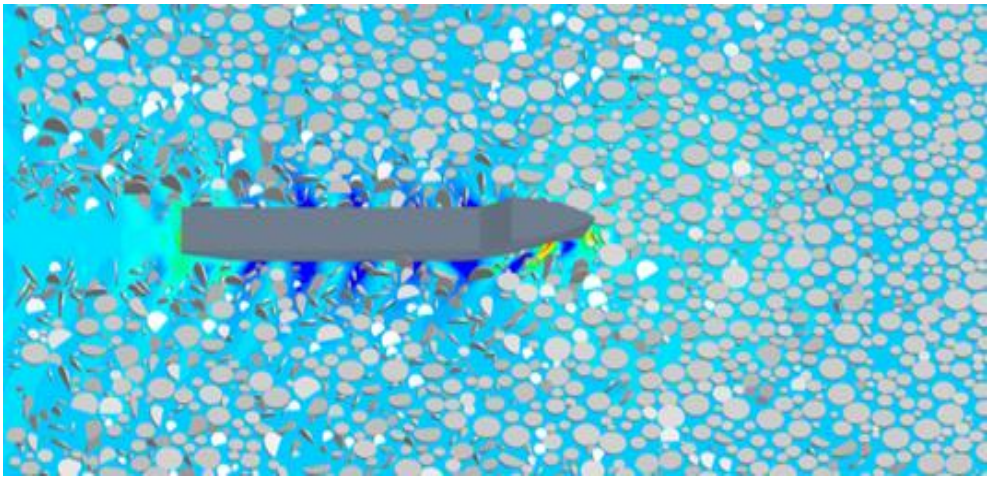

Figure 4: CFD-DEM simulation of a ship advancing in floating ice floes [33]

In this paper, an Arctic Ship Performance Model (subsequently referred to as ASPM) is designed and tested. It combines a set of classic naval architecture methods with the method of Huang et al. as well as the FSICR, providing adequate coverage of the common Arctic shipping scenarios. The model has also included the calculation of ship propulsion and fuel consumption to enable direct usage. Section 2 presents the calculation methods used. Section 3 introduces how those methods were implemented in MATLAB and presents a simple machine learning procedure for data training, regression and model selection. In Section 4, the APSM is used to simulate a previous voyage of an Arctic cargo ship across the NSR. The fuel consumption prediction of APSM agrees well with the field data collected by the ship. Finally, Section 5 concludes the work with its implications and indicates the limitation and future work.

2. Calculation methods

The ship resistance in this ASPM is treated as being composed of calm water resistance, added resistance due to wind, added resistance due to waves, and added resistance due to ice. The effects of any water current are incorporated as a loss of ship speed. The resistance is then used to calculate the required thrust at the target speed. The RPM of the propeller required to produce this thrust is then found. Next, the propulsion efficiency is calculated for the RPM and ship speed, followed by the required engine power. Finally. The fuel consumption is calculated.

2.1 Ice resistance

In the ASPM, ice resistance is classified into large ice floes and small ice floes. These two conditions correspond to significantly different physics during the ship-ice interactions. Large ice floes undergo crushing and break-up during their interaction with ships, and the ultimate of this case is level ice. By contrast, small ice floes have a high degree of freedom, thus their response to ships is mainly being pushed away rather than fractured. Extreme ice conditions, such as ice ridges, are not considered in the ASPM, since they are designed to be detected by the crew and avoided during operations. Therefore, two different methods were required to account for the ice resistance in large and small ice-floe scenarios.

The resistance calculation for large ice floes has a similar nature to that for level ice resistance, as the ship is expected to break the large floes. However, as the large floes are not continuous, equivalent ice thickness (ice thickness times ice concentration) is applied to account for the ice concentration, instead of only considering the ice thickness. This practice is further introduced by Milaković et al. [35]. Therefore, for large ice floes, the formulae provided in the Finish-Swedish Ice Class Rules (FSICR) is employed, where the method may account for large ice floes by applying the equivalent ice thickness [36], $h_E = C \times h$ (equivalent level ice thickness equals ice concentration times ice thickness).

The empirical equations to account for the ice resistance induced by large ice floes are given below [37]:

$$R_i = C_1 + C_2 v \tag{1}$$

$$C_1 = f_1\left(\frac{BL_{par}h_E}{\frac{2T}{B}+1}\right) + (1+0.021\phi)(f_2 B h_E^2 + f_3 L_{bow} h_E^2 + f_4 B L_{bow} h_E) \tag{2}$$

$$C_2 = (1+0.063\phi)\left(g_1 h_E^{1.5} + g_2 B h_E\right) + g_3 h_E\left(1+\frac{1.2T}{B}\right)\left(\frac{B^2}{\sqrt{L}}\right) \tag{3}$$

where h_E is equivalent ice thickness, B is ship beam, T is ship draught, L is ship length (between perpendiculars), L_{par} is the length of the parallel midbody at waterline, L_{bow} is the length of the foreship at waterline and ϕ is the stem angle at centerline. The coefficient values are: $f_1 = 0.23$, $g_1 = 18.9$, $f_2 = 4.58$, $g_2 = 0.67$, $f_3 = 1.47$, $g_3 = 1.55$, $f_4 = 0.29$.

For small ice floes, the empirical equation provided by Huang et al. [38] is applied. The inputs and the empirical equation are given in Equation (4).

$$R_{ice} = 0.13665 \times \gamma \times \cos\alpha \times \rho_{ice} \times h \times D \times V^2 \times B/L_{pp} \times C^{1.5} \times Fr^{-0.8} \quad (4)$$

where α & γ are ship waterline angle and ship buttock angle ice resistance coefficients that can vary with the specific ship, ρ_{ice} is ice density, B is ship beam, h is ice thickness, D is the average ice floe diameter, V is ship speed, C is the ice concentration and Fr is the Froude number. In reality, ice floes in a given region are of different dimensions, where h has little variation while D of floes can be notably different. Thus, it is recommended to input a constant h and calculate an average D for the equation based on an average Aspect Ratio (AR), i.e. $D = h \times AR$. Field measurements reported that a generally applicable average value for AR is 10 for ice floe fields [39]. The density of the ice, ρ_{ice}, can be held constant at 900 kg/m^3.

The threshold between large and small floes in the current ASPM is $C \times h = 0.3m$, which is based upon the classification of UK Met Office that when $C \times h > 0.3m$ first-year ice starts to grow and ship-induced fracture is expected occur, and when $C \times h \leq 0.3m$ ice types are young grey, pancake and grease floes that do not expect ship-induced fracture [40].

2.2 Calm-water resistance

The bare hull ship resistance was estimated using the methods presented by Holtrop & Mennen [41,42]. The Holtrop and Mennen method is widely used and generally seen to provide a good estimate of ship resistance for a wide range of ship types. This makes it a particularly good choice for an Arctic Ship Performance Model as the hullforms of ships transiting the Arctic can range from less common icebreaker forms through high displacement bulk carrier hullforms to fast container ship forms. The robustness and broad applicability of the Holtrop and Mennen method gives the flexibility to take into account this range of ship types.

The method implemented in this work defines resistance as being made up of the following components:

$$R_T = R_F(1 + k_1) + R_W + R_B + R_{TR} + R_A \quad (5)$$

where R_T is total resistance, $R_F(1+k_1)$ is viscous resistance, R_W is wave-making resistance, R_B is the change in resistance due to the presence of a bulbous bow, R_{TR} is the change in resistance due to the transom, and R_A is the model-ship correlation resistance. In this work, appendage resistance was considered negligible and so has not been included. The full equations for calculating these various calm water resistance components are lengthy and are available in [41,42].

2.3 Added resistance due to weather

Added resistance due to the environmental conditions is made up of three parts if ice is treated separately. Added resistance due to wind, added resistance due to waves, and speed loss due to current. The speed loss due to current excludes any resistance that may be caused by steering to a course or other effects, but it is proposed that this is a reasonable approximation.

Added resistance in waves is the increase in resistance caused by a ship making headway in a sea state compare to the resistance at the same speed in calm water. In this instance, it was estimated using the method presented by Liu and Papanikolaou [43]. The components of the added wave resistance are as follows:

$$R_{wave} = R_{AWM} + R_{AWR} \quad (6)$$

where R_{wave} is the total added resistance due to waves, R_{AWM} is the resistance due to ship motion effects, and R_{AWR} is the resistance due to wave reflection effects.

As the original method presented by Liu and Papanikolaou [43] was intended only for head waves, it has the tendency to over predict the added resistance due to waves for other wave directions. The following simple correction was applied:

$$R_{wave\ corrected} = R_{wave}\ cos^2 \psi \quad (7)$$

where ψ is wave angle, R_{wave} is uncorrected wave resistance and $R_{wave\ corrected}$ is the wave resistance corrected for wave angle.

Added resistance due to wind was estimated using a method recommended by the ITTC [44] and first published by Fujiwara [45] where the full set of equations used are available.

The effects of current were viewed as simply a change in target speed. The speed loss due to current was calculated as follows:

$$Speed\ loss = V_{current} \times cos\ (\theta_{current}) \tag{8}$$

where $V_{current}$ is the current speed and $\vartheta_{current}$ is the current angle.

2.4 Propulsion

The propulsive efficiency for each speed was calculated as follows. First, the required thrust is found based on the thrust deduction factor and ship resistance. The operating RPM required to produce this thrust was then found by searching for the RPM where the required thrust equals the produced thrust. In this implementation, a Newton method was used to minimise the difference between required and produced thrust. The RPM at this minimum was taken as the operating RPM for a given speed and set of environmental conditions.

In order to calculate the thrust, the following methods and formulae were used. Firstly, the thrust deduction factor was calculated using the approximation from [41].

$$t = \frac{0.25014\left(\frac{B}{L}\right)^{0.28956}\left(\sqrt{\frac{BT}{D}}\right)^{0.2624}}{\left(1 - C_p + 0.0225\ LCB\right)^{0.01762}} + 0.0015\ C_{stern} \tag{9}$$

where B is waterline beam, L is waterline length, T is moulded draft, D is depth, C_p is a prismatic coefficient, LCB is the longitudinal centre of buoyancy forward of midships, and C_{stern} is a coefficient based on the stern shape.

Open water efficiency was found in the standard way using:

$$\eta_O = \frac{JK_T}{2\pi K_Q} \tag{10}$$

The KT and KQ values were calculated using the interpolated values for a Wageningen B Series propeller published by Oosterveld and van Oossanen (1975). The main equations are below and the full sets of published coefficients can be found in the original publication.

$$K_T = \sum_{n=1}^{39} C_n (J)^{s_n} \left(\frac{P}{D}\right)^{t_n} \left(\frac{A_E}{A_0}\right)^{u_n} (z)^{v_n} \quad (11)$$

$$K_Q = \sum_{n=1}^{47} C_n (J)^{s_n} \left(\frac{P}{D}\right)^{t_n} \left(\frac{A_E}{A_0}\right)^{u_n} (z)^{v_n} \quad (12)$$

where P/D is the pitch diameter ratio, A_E/A_0 is the blade area ratio, z is the number of blades, and the remaining coefficients are given in [46].

J was calculated in the standard way using:

$$J = \frac{V_a}{nD} \quad (13)$$

where V_a is the advance speed, n is the propeller revolutions per second, and D is the propeller diameter.

$$\eta_R = 0.9922 - 0.05908(BAR) + 0.07424(C_p - 0.0225LCB) \quad (14)$$

where LCB is the position of the longitudinal centre of buoyancy forward of $0.5L$ as a percentage of L, C_P is the prismatic coefficient, and BAR is the propeller blade area ratio.

The wake fraction was found using Taylor's method, and then the hull efficiency was found using the previously calculated thrust deduction factor along with this wake fraction.

$$w_T = 0.5\, C_B - 0.05 \quad (15)$$

$$\eta_H = \frac{1 - t}{1 - w_T} \quad (16)$$

where η_H is the hull efficiency, t is the thrust deduction factor, and w_T is the wake fraction. Finally, the required engine power is found using:

$$P_R = V \cdot R_T \cdot \eta_R \eta_H \eta_O \quad (17)$$

where the efficiencies are as previously defined, P_R is the required engine power, R_T is the total resistance as previously defined, and V is the ship speed.

2.5 Fuel consumption

Fuel consumption was calculated based on the procedure laid out in the MAN B&W Principles of Ship Propulsion Guide [47]. With this method, fuel consumption is calculated based on the engine manufacturer's data. These provide specific fuel consumption results for different loading conditions as shown in Table 1.

Table 1: Engine loading conditions and the corresponding fuel consumption results.

Engine speed	124 rpm		95 rpm	
Full load, rating point	R1	R2	R3	R4
Output (kW)	10470	7980	8040	6120
Brake specific fuel consumption (g/kWh)	168.8	162.8	168.8	162.8

3. Implementation in MATLAB

The ASPM was integrated into MATLAB. To improve the speed of the ship performance prediction, a response surface representation of the ASPM was used. These response surfaces were trained on outputs from the ASPM as is further detailed in Section 3.2. Although there is a tradeoff made by using a response surface model rather than direct calculation of the ship performance, it is proposed that the loss of accuracy is minimal and appropriate for the case study under consideration; it is also proposed that the benefit of a speedup in calculation time justifies the use of a response surface in this case.

3.1 Response surface modelling

The ASPM can be run for a specific ship and its voyage condition to obtain a response surface. The response surface consists of results from numerous data points, i.e. using discrete data to form a continuous range. Within the intended response surface range, the data points are randomly generated until a reliable response surface is established that also covers the data points that are not trained.

As a demonstration of this study, two response surfaces were trained. The inputs for response surface 1 are ship target speed, wind speed, wind direction, significant wave height, wave direction, current speed,

current direction, ice concentration, and ice thickness. The output for this response surface is required engine power. For response surface 2, the input is engine power, and the output is fuel consumption. The reason for splitting the response surface model into two was first and foremost to allow for the maximum achievable speed to be searched for if the required power for a given target speed is higher than the installed power.

3.2 Regression model training and selection

The calculation methods outlined in Section 2 were implemented and a set of training data was generated by creating 2000 random samples using uniformly distributed random values as input for the operational parameters covering the full range present in the input matrix X for this case study. The data was then loaded into MATLAB and several different regression methods were tested using the MATLAB Regression Learner App. Validation of the models was performed using cross-validation with ten folds. The route's mean squared error was used as the metric to judge the quality of each regression method. The results of this study are shown in Table 2 and Table 3 with the results for the selected models highlighted in green. It should be noted that the prediction speed is for comparison purposes only and the response surface models will run at different speeds on different computers.

Table 2: Results from regression model comparison for response surface 1

Group	Model	Route mean squared error (kW)	R-squared	Mean squared error (kW^2)	Mean absolute error (kW)	Prediction speed (obs/sec)
Linear regression	Linear	10115	0.76	1.0231e+08	8286.3	140000
	Interactions linear	10097	0.76	1.0195e+08	8284.9	110000
	Robust linear	10748	0.73	1.1552e+08	7676	140000
	Stepwise linear	10098	0.76	1.0196e+08	8288.1	130000
Tree	Fine tree	548.84	1.00	3.0123e+05	368.1	210000
	Medium tree	725.33	1.00	5.2611e+05	462.51	280000
	Coarse tree	1211.8	1.00	1.4685e+06	766.41	310000
Support Vector Machine (SVM)	Linear SVM	11511	0.69	1.325e+08	7550.3	73000
	Quadratic SVM	4080.7	0.96	1.6652e+07	2871.3	110000
	Cubic SVM	1207.1	1.00	1.4571e+06	1080.3	210000
	Fine Gaussian SVM	4151.1	0.96	1.7232e+07	2450	85000
	Medium Gaussian SVM	1417.5	1.00	2.0093e+06	1057.4	160000
	Coarse Gaussian SVM	5032.9	0.94	2.533e+07	2988.3	74000
Ensemble	Boosted trees	1402.3	1.00	1.9665e+06	907.7	47000
	Bagged trees	1388.1	1.00	1.9269e+06	673.54	29000

Gaussian process regression (GPR)	Squared exponential GPR	173.33	1.00	30043	103.26	24000
	Exponential GPR	522.69	1.00	2.732e+05	216.38	18000
	Rational quadratic GPR	172.95	1.00	29910	102.51	13000

305

306 Table 3: Results for regression model comparison for response surface 2

Group	**Model**	**Route mean squared error (tonnes/day)**	**R-squared**	**Mean squared error ([tonnes/day]^2)**	**Mean absolute error (tonnes/day)**	**Prediction speed (obs/sec)**
Linear regression	Linear	0.76224	1.00	0.58101	0.50636	170000
	Interactions linear	0.76224	1.00	0.58101	0.50636	170000
	Robust linear	0.9289	1.00	0.86286	0.45113	180000
	Stepwise linear	0.76224	1.00	0.58101	0.50636	170000
Tree	Fine tree	0.38834	1.00	0.15081	0.28712	340000
	Medium tree	0.39638	1.00	0.15712	0.29025	330000
	Coarse tree	0.88971	1.00	0.79159	0.53006	380000
Support Vector Machine (SVM)	Linear SVM	5.0949	0.99	25.958	4.6283	320000
	Quadratic SVM	5.2188	0.99	27.236	4.7815	310000
	Cubic SVM	8.1926	0.98	67.118	6.6501	310000
	Fine Gaussian SVM	5.6972	0.99	32.458	5.3492	320000
	Medium Gaussian SVM	4.5653	0.99	20.842	3.9541	260000
	Coarse Gaussian SVM	4.2216	1.00	17.822	3.4301	300000
Ensemble	Boosted trees	3.6298	1.00	13.175	2.5934	53000
	Bagged trees	0.16401	1.00	0.0269	0.11823	42000
Gaussian process regression (GPR)	Squared exponential GPR	0.030135	1.00	0.00090811	0.023335	27000
	Exponential GPR	0.0025498	1.00	6.5016e-06	0.00034901	19000
	Rational quadratic GPR	0.022476	1.00	0.00050517	0.016434	14000

307

308 The results show that prediction speed is good for both response surfaces (Tables 2 and 3), with none
309 of the modelling methods performing poorly in this regard, although there is an apparent tradeoff
310 between prediction error and speed. The mean absolute error for response surface 1 (Table 2) ranges
311 from 8288.1 kW to 102.51 kW, the upper end of this range is unacceptably high given the MCR of the
312 engine is 10470 kW, but the lower end is acceptable for this work, representing 0.98% of the MCR.
313 The mean absolute error for response surface 2 (Table 3) ranges from 6.6501 to 0.00349 tonnes/day.
314 The fuel consumption is usually around 0.8 tonnes/hour (as will be shown in the full-scale measurement
315 of the next section, Figure 8), making the lower end of this range of errors very acceptable, however,
316 the higher end of this range would represent over eight hours of normal fuel consumption, which is an

unacceptably high error. In order to make sure the high-error region does not cover a normal operation condition, the following analyses are made:

Based on the results of the regression model comparison, the two models selected were the rational quadratic Gaussian process regression for the model predicting required power (response surface 1), and the exponential Gaussian process model for the prediction of fuel consumption from power (response surface 2). This selection was based on the route mean squared error (RMSE) values.

The residuals for response surface 1 presented in Figure 5 show a higher error for predicted power at high speeds. As these high speeds were not achieved for this case study, this is not of great concern. The speeds of greatest interest are 11-13.5 knots, and at these speeds the error is only a small proportion of the actual target power. This level of error has little effect on the fuel consumption prediction. It is likely this higher error at high speeds is due to fewer training data points in this region. The density of points in the training data is much greater at lower engine power resulting in a better model fit where there is a high density of training data.

The residuals for response surface 2, shown in Figure 6, report the greatest error as engine power approaches zero. For a regression method that is used here, the mathematical function normally multiplies different parameters together, with coefficients and exponents added for each. Therefore, when the achieved power is almost zero, the output of the function approaches zero (shows as excessively small). Whilst keeping the function accurate for the whole intentional range, normally there is no need to correct these nearly zero points, as they are also not a realistic operation condition.

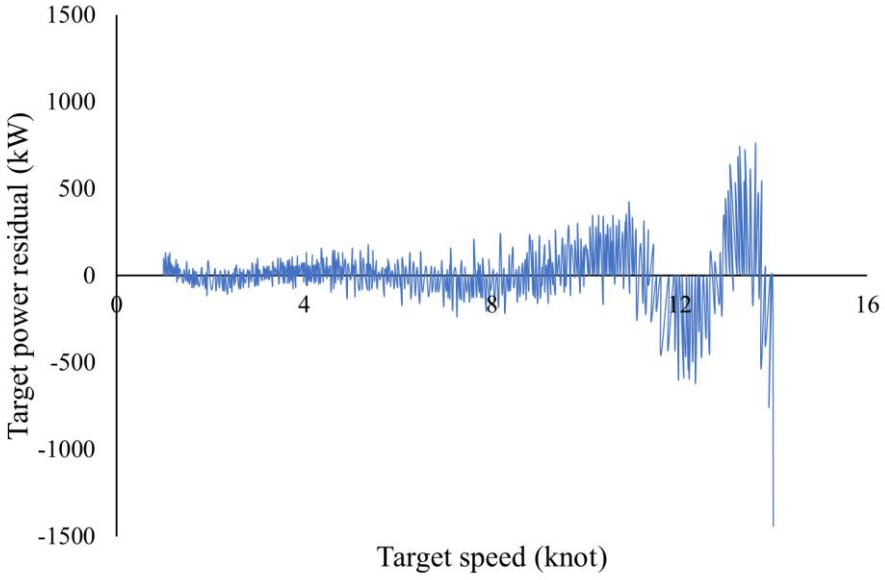

Figure 5: Residuals plot for the speed to power Rational Quadratic Gaussian Process model response surface

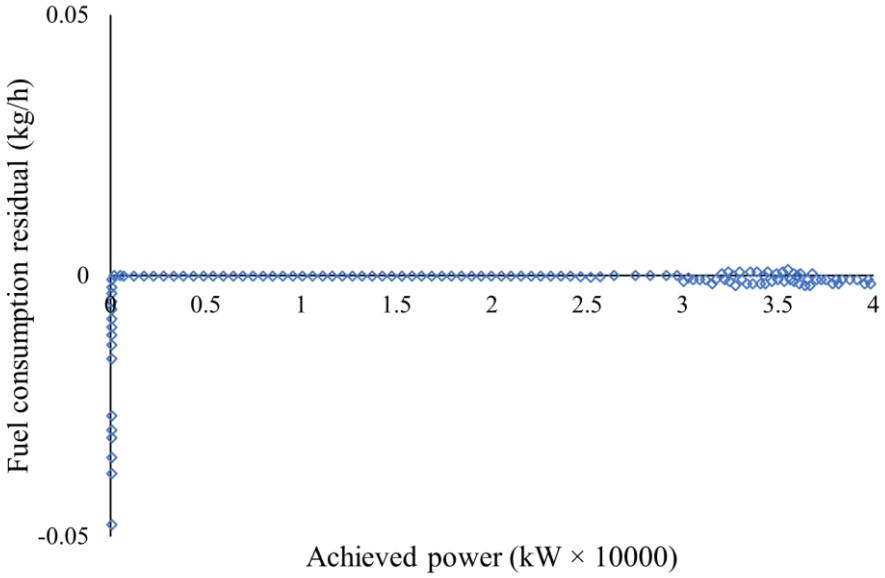

Figure 6: Residuals plot for the power to fuel consumption Exponential Gaussian Process model response surface

4. Validation

4.1 Case study vessel and voyage

The case study ship used in this work is an in-service Arctic cargo ship. The reason for using this case study ship was to compare the model results with full-scale measurements for a voyage along the NSR. The voyage was carried out between 25/07/2018 19:00 to 14/08/2018 13:00, from Port Shanghai in China to Port Gothenburg in Sweden. The collected data include ship speed, GPS location, encountered wind and fuel consumption. Other encountered environmental parameters such as ocean current, water temperature, and bathymetry were not recorded onboard, while they were found in the weather record database by selecting the corresponding time and locations. Specifically, Metocean data for ocean current and water temperature are from the Copernicus Marine Environment Monitoring Service (CMEMS), while bathymetry data are obtained from the International Bathymetric Chart of the Arctic ocean (IBCAO). Sea ice data are from the satellite record of the UK Met Office. Figure 7 shows the encountered wave and sea ice conditions.

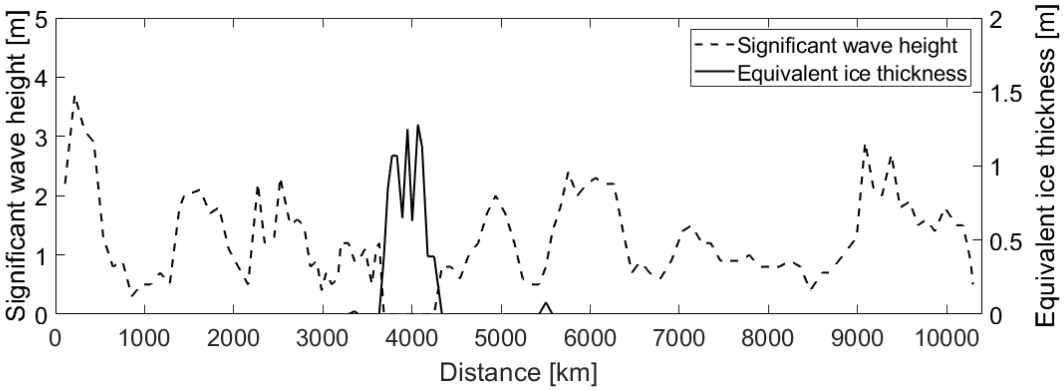

Figure 7: The encountered significant wave height and the Equivalent ice thickness

This particular voyage was replicated using the ASPM, where the above data were inputted, together with particulars of the in-service Arctic cargo ship. The ship particulars are: overall shiplength 190 m, midship breadth 28.5 m, midship depth 15.8 m, scantling draft 11.0 m, deadweight 37124.8 tonnes, and FSICR Ice Class 1A. The propulsion system uses the engine type WinGD 6RT-flex50-D, which has a Maximum Continuous Rating (CSR) 10,470kW * 124 r/min and Continuous Synopsis Record = 65% MCR. The designed service speed of the ship is 14.8 knots.

4.2 Comparison of fuel consumption

The ASPM was used to calculate the fuel consumption of every data point as per the introduced voyage. Figure 8 presents the fuel consumption comparison between the ASPM and the measurement. It is seen that the prediction of ASPM agrees reasonably well with the measurement, with changes in fuel consumption due to weather and sea ice conditions corresponding well. From Figure 8, it is seen that the fuel consumption increases sharply when ice is encountered, which confirms that the ice resistance dominates in the total ship resistance even though the ice fields are not consolidated. Noting that the fuel consumption dramatically declined before the vessel entered the Arctic waters, this was nevertheless due to the voluntary speed reduction of the ship crew, which is a common practice.

The certain deviation of fuel consumption could be due to several reasons. Firstly, the ship performance model is based on the methods presented by Holtrop and Mennen [41] which were derived from performance data of ships in the 1980s. Ship design has moved on since then, and energy efficiency has become a greater focus for naval architects, resulting in different performance profiles in contemporary vessels. Secondly, there are several assumptions around the propeller type, the ASPM assumed a Wageningen B Series, which may be less efficient than the installed propeller. Thirdly, the model was run at constant target speeds on dedicated legs, which was to try and reconcile the fact that the model implements a constant target speed and the actual vessel is operated at a constant RPM, but this may have introduced additional errors. Despite these discrepancies, the overall agreement of fuel

consumption prediction can justify that the selected theories in the ASPM are reasonable, they have been correctly implemented in the code, and the response surface was built effectively via the Machine Learning functions.

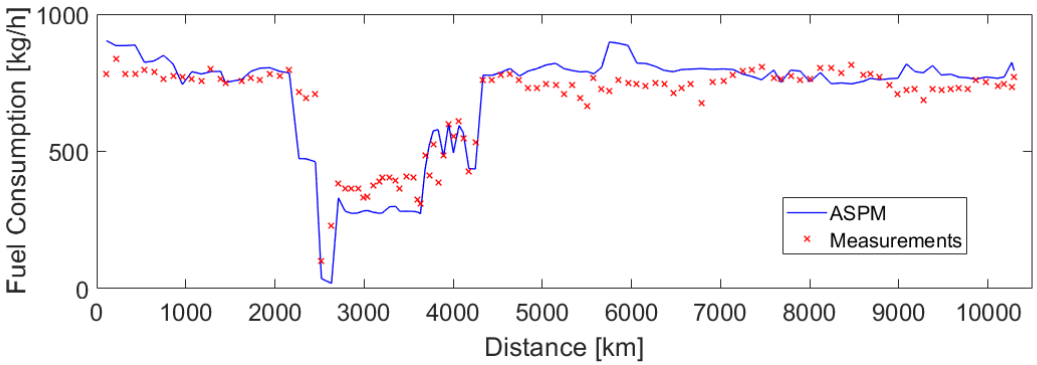

Figure 8: Comparison of fuel consumption between predicted by ASPM and measured during the actual journey

5. Conclusions

This work has presented a ship performance model for use in the context of Arctic shipping which makes use of classical naval architecture methods alongside a novel ice resistance prediction algorithm. The integration of these methods into a coherent Arctic Ship Performance Model, and subsequently validation against full-scale measurement has demonstrated that the model performs well for predicting fuel consumption for a completed journey of an Arctic specific vessel via the Northern Sea Route.

By combining the classical naval architecture methods with machine learning tools and techniques for building response surfaces such as those provided by MATLAB, it has been shown that the development process can be sped up and result in faster more performant response surfaces. These response surfaces are well suited for integration into a wide range of tools to support decision making for both ship design and operations.

There are still some limitations in the ASPM as discussed. Corresponding future work includes updating some old naval architecture approaches to better fit modern hull forms, improvement of the ice resistance model for different ice conditions, further validation using data from future voyages where a broader variety of ice conditions were encountered, and finally, releasing as much of the code as possible as an open-source package.

Acknowledgements

This work is part of a project that has received funding from the European Union's Horizon 2020 research and innovation programme under grant agreement No 723526 - SEDNA: Safe maritime operations under extreme conditions; the Arctic case.

References

[1] C. Ørts Hansen, P. Grønsedt, C. Lindstrøm Graversen, C. Hendriksen, Arctic shipping–commercial opportunities and challenges, Copenhagen Business School Maritime. (2016).
[2] A. Monitoring, Changes in arctic snow, water, ice and permafrost. swipa 2011 overview report, Arctic Climate. (2012).
[3] Z. Li, J.W. Ringsberg, F. Rita, A voyage planning tool for ships sailing between Europe and Asia via the Arctic, Ships and Offshore Structures. 15 (2020) S10–S19.
[4] Z. Li, C. Ryan, L. Huang, L. Ding, J.W. Ringsberg, G. Thomas, A comparison of two ship performance models against full-scale measurements on a cargo ship on the Northern Sea Route, Ships and Offshore Structures. (2021). https://doi.org/10.1080/17445302.2021.1926146.
[5] J.N. Calleya, Ship design decision support for a carbon dioxide constrained future, PhD Thesis, UCL (University College London), 2014.
[6] F. Tillig, Simulation model of a ship's energy performance and transportation costs, PhD Thesis, Chalmers University of Technology, 2020.
[7] E. Enkvist, On the ice resistance encountered by ships operating in the continuous mode of icebreaking, 1972.
[8] A. Lindquist, Straightforward method for calculation of ice resistance of ships, POAC'89. (1989).
[9] K. Riska, Performance of merchant vessels in ice in the Baltic, Sjöfartsverket, 1997.
[10] M. Juva, K. Riska, On the power requirement in the Finnish-Swedish ice class rules, Winter Navigation Research Board, Res. Rpt. 53 (2002).
[11] J. Thomson, S. Ackley, F. Girard-Ardhuin, F. Ardhuin, A. Babanin, G. Boutin, J. Brozena, S. Cheng, C. Collins, M. Doble, Overview of the arctic sea state and boundary layer physics program, Journal of Geophysical Research: Oceans. (2018).
[12] V.C. Khon, I.I. Mokhov, M. Latif, V.A. Semenov, W. Park, Perspectives of Northern Sea Route and Northwest Passage in the twenty-first century, Climatic Change. 100 (2010) 757–768.
[13] Reuters, As Arctic Ice Melts, Polluting Ships Stream Into Polar Waters, GCaption. (2020).
[14] A. Polojärvi, J. Tuhkuri, O. Korkalo, Comparison and analysis of experimental and virtual laboratory scale punch through tests, Cold Regions Science and Technology. 81 (2012) 11–25.
[15] C. Guo, C. Xie, J. Zhang, S. Wang, D. Zhao, Experimental Investigation of the Resistance Performance and Heave and Pitch Motions of Ice-Going Container Ship Under Pack Ice Conditions, China Ocean Eng. 32 (2018) 169–178. https://doi.org/10.1007/s13344-018-0018-9.
[16] W.-Z. Luo, C.-Y. Guo, T.-C. Wu, Y.-M. Su, Experimental research on resistance and motion attitude variation of ship–wave–ice interaction in marginal ice zones, Marine Structures. 58 (2018) 399–415. https://doi.org/10.1016/j.marstruc.2017.12.013.
[17] B. Yang, Z. Sun, G. Zhang, Q. Wang, Z. Zong, Z. Li, Numerical estimation of ship resistance in broken ice and investigation on the effect of floe geometry, Marine Structures. 75 (2021) 102867.
[18] J.-H. Kim, Y. Kim, H.-S. Kim, S.-Y. Jeong, Numerical simulation of ice impacts on ship hulls in broken ice fields, Ocean Engineering. 180 (2019) 162–174.
[19] S.-Y. Jeong, K. Choi, H.-S. Kim, Investigation of ship resistance characteristics under pack ice conditions, Ocean Engineering. 219 (2021) 108264.
[20] D.B. Colbourne, Scaling pack ice and iceberg loads on moored ship shapes, Oceanic Engineering International. 4 (2000) 39–45.
[21] R.C. Woolgar, D.B. Colbourne, Effects of hull–ice friction coefficient on predictions of pack ice forces for moored offshore vessels, Ocean Engineering. 37 (2010) 296–303.

[22] E.H. Hansen, S. Løset, Modelling floating offshore units moored in broken ice: comparing simulations with ice tank tests, Cold Regions Science and Technology. 29 (1999) 107–119.
[23] M. Lau, K.P. Lawrence, L. Rothenburg, Discrete element analysis of ice loads on ships and structures, Ships and Offshore Structures. 6 (2011) 211–221.
[24] S. Ji, Z. Li, C. Li, J. Shang, Discrete element modeling of ice loads on ship hulls in broken ice fields, Acta Oceanologica Sinica. 32 (2013) 50–58.
[25] J. Wang, A. Derradji-Aouat, Ship performance in broken ice floes-preliminary numerical simulations. Newfoundland: Institute for Ocean Technology (IOT) Report No, TR-2010-24, 2010.
[26] J. Wang, A. Derradji-Aouat, Numerical assessment for stationary structure (Kulluk) in moving broken ice, in: Proceedings of the International Conference on Port and Ocean Engineering Under Arctic Conditions, 2011.
[27] R. Lubbad, S. Løset, W. Lu, A. Tsarau, M. van den Berg, An overview of the Oden Arctic Technology Research Cruise 2015 (OATRC2015) and numerical simulations performed with SAMS driven by data collected during the cruise, Cold Regions Science and Technology. 156 (2018) 1–22.
[28] J. Tuhkuri, A. Polojärvi, A review of discrete element simulation of ice–structure interaction, Philosophical Transactions. Series A, Mathematical, Physical, and Engineering Sciences. 376 (2018).
[29] L.J. Yiew, L.G. Bennetts, M.H. Meylan, G.A. Thomas, B.J. French, Wave-induced collisions of thin floating disks, Physics of Fluids. 29 (2017) 127102. https://doi.org/10.1063/1.5003310.
[30] L. Huang, G. Thomas, Simulation of Wave Interaction With a Circular Ice Floe, Journal of Offshore Mechanics and Arctic Engineering. 141 (2019) 041302.
[31] L. Huang, K. Ren, M. Li, Ž. Tuković, P. Cardiff, G. Thomas, Fluid-structure interaction of a large ice sheet in waves, Ocean Engineering. 182 (2019) 102–111.
[32] L. Huang, M. Li, T. Romu, A. Dolatshah, G. Thomas, Simulation of a ship operating in an open-water ice channel, Ships and Offshore Structures. 0 (2020) 1–10. https://doi.org/10.1080/17445302.2020.1729595.
[33] L. Huang, J. Tuhkuri, B. Igrec, M. Li, D. Stagonas, A. Toffoli, P. Cardiff, G. Thomas, Ship resistance when operating in floating ice floes: A combined CFD&DEM approach, Marine Structures. 74 (2020) 102817.
[34] L. Huang, Z. Li, C. Ryan, M. Li, J. Ringsberg, B. Igrec, G. Andrea, D. Stagonas, G. Thomas, Ship Resistance When Operating in Floating Ice Floes: a Derivation of Empirical Equations, in: ASME 2020 39th International Conference on Ocean, Offshore and Arctic Engineering (OMAE), 2020.
[35] A.-S. Milaković, F. Li, R.U.F. von Bock und Polach, S. Ehlers, Equivalent ice thickness in ship ice transit simulations: overview of existing definitions and proposition of an improved one, Ship Technology Research. 67 (2020) 84–100.
[36] A. Keinonen, R. Browne, A. Reynolds, Icebreaker Characteristics Synthesis, 1996.
[37] K. Riska, M. Wilhelmson, K. Englund, T. Leiviskä, Performance of Merchant vessels in the Baltic, Ship Laboratory, Winter Navigation Research Board, Helsinki University of Technology, Espoo, Finland, Research Report. (1997).
[38] L. Huang, Z. Li, C. Ryan, J.W. Ringsberg, B. Pena, M. Li, L. Ding, G. Thomas, Ship resistance when operating in floating ice floes: Derivation, validation, and application of an empirical equation, Marine Structures. 79 (2021) 103057.
[39] A. Alberello, M. Onorato, L. Bennetts, M. Vichi, C. Eayrs, K. MacHutchon, A. Toffoli, Brief communication: Pancake ice floe size distribution during the winter expansion of the Antarctic marginal ice zone, The Cryosphere. 13 (2019) 41–48.
[40] N. Fournier, Sea ice type classification for ship performance modelling, UK Met Office, 2019.
[41] J. Holtrop, G.G.J. Mennen, An approximate power prediction method, International Shipbuilding Progress. 29 (1982) 166–170.
[42] J. Holtrop, A statistical re-analysis of resistance and propulsion data, International Shipbuilding Progress. 31 (1984) 272–276.
[43] S. Liu, A. Papanikolaou, Fast approach to the estimation of the added resistance of ships in head waves, Ocean Engineering. 112 (2016) 211–225.
[44] ITTC, Analysis of Speed/Power Trial Data, ITTC Report. (2014).

517 [45] T. Fujiwara, A New Estimation Method of Wind Forces and Moments Acting on Ships on the
518 Basis of Physical Components Models, Journal of the Japan Society of Naval Architects and
519 Ocean Engineers. 2 (2006) 243–255.
520 [46] M.W.C. Oosterveld, P. van Oossanen, Further computer-analyzed data of the Wageningen B-
521 screw series, International Shipbuilding Progress. 22 (1975) 251–262.
522 [47] MAN, Two-Stroke Project Guides [https://marine.man-es.com/two-stroke/project-guides],
523 Project Guides and Engine Selection Guides. (2019).
524